*J. Fluid Mech.* (1997), *vol.* 330, *pp.* 189–213



# Stability of slender liquid bridges subjected to axial flows

By BRIAN J. LOWRY† AND PAUL H. STEEN

School of Chemical Engineering and Center for Applied Mathematics, Cornell University, Ithaca, NY 14853-5204, USA

(Received 23 June 1995 and in revised form 26 July 1996)

Experiments document the influence of flow on the Plateau–Rayleigh (PR) instability of a near-cylindrical liquid bridge. The slightly heavy bridge is subjected to a surrounding pipe flow from bottom to top. Linear and nonlinear regimes of response are reported. Islands of stability in flow rate are observed; that is, there are bridges that are stable with flow but otherwise not. Density imbalance and flow each, on its own, is destabilizing but together they are stabilizing as recorded by a variety of measures. This nonlinear stabilization is explained in terms of the codimension-2 nature of the pitchfork bifurcation of the 'perfect' Plateau–Rayleigh instability.

## 1. Introduction

Instabilities driven by surface tension are favoured when surface areas are large relative to volumes (small length scales) or when gravity is reduced (low gravity). Plateau used both a soap film (small film thickness) and density-matched liquids (low-gravity simulation) in his experimental studies of the figures of equilibrium of liquid masses (Plateau 1863, 1873). The influence of flow on the stability of shapes is our focus and density-matched liquids are used in our apparatus, sometimes referred to as a Plateau chamber.

The simplest surface-tension-driven instability, for disturbances that preserve volume, occurs for a cylinder of motionless liquid. Cylinders longer than their circumference are unstable. Length equal to circumference is called the Plateau–Rayleigh (PR) stability limit. The instability can be understood in terms of the Young–Laplace equation. Consider small axisymmetric disturbances. The bridge shape becomes undular, with an inward neck at one end and an outward bulge at the other. For short bridges, disturbances in azimuthal curvature dominate those in radial curvature. For long bridges, the reverse is true. The crossover occurs at the PR limit beyond which pressure in the neck is greater than that in the bulge. Hence, liquid is driven from the neck into the bulge and the disturbance grows. The presence of flow either within or outside the cylinder can influence the pressure distribution and hence the instability.

In our apparatus, a liquid bridge is placed coaxially in a glass tube that is filled with an immiscible neutrally buoyant liquid. The bathing liquid can be motionless, in which case the apparatus functions as a classical Plateau chamber. On the other hand, the bathing liquid can be driven past the bridge by an axial pressure gradient, in which case the bridge is part of a larger pipe flow of considerable length.

† Present address: Department of Chemical Engineering, University of New Brunswick, Fredericton, New Brunswick, Canada E3B 5A3.

Motivation for the study comes from the fundamental level. It is desired to examine the influence of flow on capillary containment in a simple context. The competition between nonlinear effects is richest near the codimension-2 singular point corresponding to the PR bifurcation point. Such competing instabilities are relevant to a variety of scientific and technological issues: for example, thermocapillary-driven float-zone instability and fluids management in space laboratories, respectively.

An interesting twist concerns the role of density imbalance. At the outset, density imbalance was viewed as a fact of experimental reality, however unfortunate. It turns out that density imbalance is beneficial both in practice for successful experimental protocol and in theory in providing an avenue to stabilization beyond the PR limit.

In the absence of flow, the configuration of the bridge is controlled by bridge length $L$, bridge volume $V$, and the influence of gravity $B$ (Bond number). Length $L$ is scaled by the radius of the circular contact lines and $V$ by 'the cylindrical volume' (i.e. that volume enclosed by a cylindrical interface of length $L$). The experiments are restricted to volumes that are nearly cylindrical, $V \approx 1$, and gravity that is weak, $B \ll 1$. The influencing flow will be measured by the flow-induced pressure force relative to the surface tension force, $C$ (capillary number), and will be small by control, $C \ll 1$. Definitions are given below.

Steady shape is the response to steady flow up to the stability limit for low to moderate flow rates. Several regimes in the response are identified. In the no-flow case, classical liquid bridge shapes and stability are recovered. At low flow rates, shapes and curvature profiles are found to deviate from the no-flow case in a linear manner. This linear behaviour can be understood in terms of the difference between the pressure gradient induced in the bridge liquid and that in the forced flow. This difference adds linearly to the hydrostatic gradient due to any density imbalance. At greater flow rates, a nonlinear response is documented. This response is the emphasis of this paper.

Related work that uses the dynamic Plateau chamber serves as background. That pressure gradients due to flow can counter gravity and stabilize bridges to lengths that are otherwise unstable – a *linear* effect – has been previously reported in brief (Lowry & Steen 1994). A detailed description of the apparatus is also available where selected data were included as motivation (Lowry & Steen 1995*a*, where figures 7*b* and 10 appear). An account and evaluation of the digital imaging technique as applied to curvature profiles is presented in Lowry 1996*b* (where figure 9*b* appears).

This paper summarizes various experimental observations near the PR limit and makes the case for a *nonlinear* stabilizing effect of flow. It is organized as follows. An overview of the flow system is offered first. Then, a problem formulation for the cases without flow and with flow is presented, to facilitate interpretion of the experiments. Next, issues of liquid selection and measurement are described. A theoretical framework that organizes the various observations follows. Among the results, first is a description of behaviour near collapse. The remaining results are split into observation of pointwise response (curvature profile), average response (shape deviation) and stability limits (maximum length and flow rate).

## 2. Overview

A sketch of the test section of the system is shown in figure 1. The liquid bridge is captured between two rods whose ends have been machined to encourage fixed circular contact lines. It is held vertically, so that the liquid/liquid interface is axisymmetric in the absence of flow. For the experiments that we report, except for

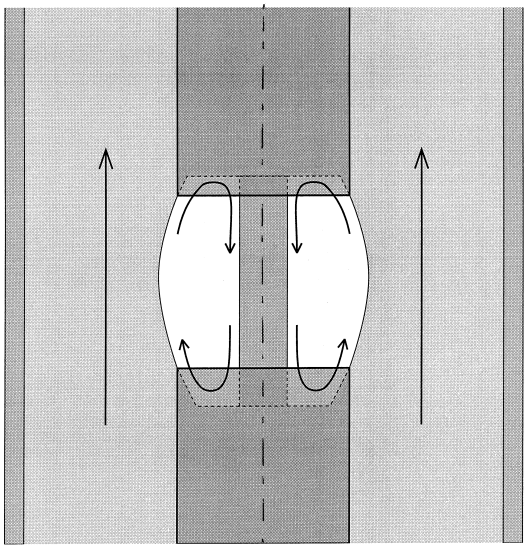

FIGURE 1. Two-fluid axisymmetric laminar flow: axial annular flow of fluid A past a cylindrical core of fluid B.

high flow rates, the shapes are also axisymmetric in the presence of flow. The top and bottom rods are connected by a centre rod of smaller diameter. In the absence of flow, the connector rod has no influence on the interface shape. The shape and its stability are determined solely by the surface energy of liquid/liquid contact area and the axial pressure field due to any buoyancy difference. In the presence of flow (typical streamlines are shown), the connector rod is crucial in providing an annular layer for lubrication pressures to develop.

This pressure is key to the phenomena observed. Suppose the bridge liquid is neutrally buoyant with respect to its bath. In the absence of flow, the pressure field on both sides of the interface is uniform, differing by a constant proportional to the mean curvature of the interface according to the Young–Laplace equation.

How will the bridge shape respond if an external flow from bottom to top is imposed (cylindrical volume, say)? The external (annular) flow is driven by a streamwise pressure gradient as in a pipe flow. The pressure drop on the pipe side of the interface is felt as a streamwise pressure rise on the bridge side. The shear stress transmitted across the interface drives a flow within the bridge that induces an additional pressure rise in the streamwise direction due to the closed ends. Depending on the viscosity contrast and the size of the connector rod, the bridge flow can dominate the pressure rise due to the external flow. The bridge shape responds as if the bridge were buoyant (i.e. it bulges upwards).

On the other hand, in the absence of flow, a bridge liquid that is heavier than its bath will bulge downward responding to the linear decrease in axial pressure with height (bridge side). The two effects can counter one another and it is expected that flow can be used to cancel density imbalance.

More interesting is what might occur near the PR limit ($L = 2\pi$). If gravity can be used to cancel the bulge-up due to flow, then flow may be able to stabilize bridges to lengths beyond the PR limit. Bridges longer than $L = 2\pi$ with cylindrical volumes may be possible. The argument goes as follows. Gravity by itself is always destabilizing in that, as the density balance is broken, the bridge bulges up or down

and becomes unstable at lengths shorter than $L = 2\pi$. The effect is the same whether the bridge is buoyant or heavy since the surface tension instability by itself is impartial to the bulge-up or bulge-down mode of growth. As described above, the effect of flow is to create an upward bulge (i.e. in flow direction) and in this way acts like density imbalance. On the other hand, flow in the bridge can be *stabilizing* in that deflections of the interface are resisted. An inward bulge tends to restrict the pressure-driven return flow which responds by pushing the interface back out. Similarly, an outward bulge is resisted by pulling the interface back inwards. These kinematic waves (standing) are the result of continuity. The idea is for flow and gravity to cancel to first order so that the stabilizing influence of the flow is left dominant at next order.

However sound the concept, there are significant hurdles to its experimental realization. First, to access the weakly nonlinear neighbourhood of the PR instability requires sufficient control of disturbances and of the 'control' parameters themselves. What 'sufficient' means is not known beforehand. How small is 'small' is one answer provided by the experiments. Second, what is convenient to control in the laboratory is not necessarily convenient for the theory that frames the phenomena. Some skill in interpretation is required.

The test section is one of three components that make up the apparatus. Upstream and downstream of the bridge are long entrance and exit regions (1 m and 0.5 m in length, respectively) that serve to maintain a laminar disturbance-free annular flow. The water flow in the tube annulus is driven by a constant pressure head tank. Bridge liquid can be injected or removed through an umbilic line in the lower rod via a tube connected to a metering pump. The bridge length is controlled by the upper rod which can be precisely moved up and down along its axis by a gear drive. The apparatus has been described in detail elsewhere (Lowry & Steen 1995*a*).

The parameters under direct experimental control are the flow rate of the external liquid $C$, and the length $L$ and volume $V$ of the bridge. Many paths connect any two states in this space. Three protocols are used in the experiments: vary $V$ with $L$ and $C$ fixed, vary $C$ with $V$ and $L$ fixed, and vary $L$ maintaining $V = 1$ with $C$ fixed. Curvature profiles and shape deviation are typically measured as dependent variables in the first protocol. Maximum flow rates and lengths (i.e. those at which the bridge breaks) are measured in the second and third protocols.

## 3. Formulation

### 3.1. *No-flow case*

For near-cylindrical volumes (with or without gravity), the shape of the bridge is axisymmetric. It may be determined by solving the Young–Laplace equation:

$$[p] \quad = \quad \bar{\kappa} = \bar{\kappa}_0 - Bz, \tag{3.1}$$

where

$$\left.\begin{aligned} \bar{\kappa} &\equiv \kappa_1 + \kappa_2, \\ \kappa_1 &\equiv \text{axial curvature}, \\ \kappa_2 &\equiv \text{radial curvature} \equiv \dot{z}/r, \\ \ddot{r} &= -\kappa_1 \dot{z}, \\ \ddot{z} &= +\kappa_1 \dot{r}. \end{aligned}\right\} \tag{3.2}$$

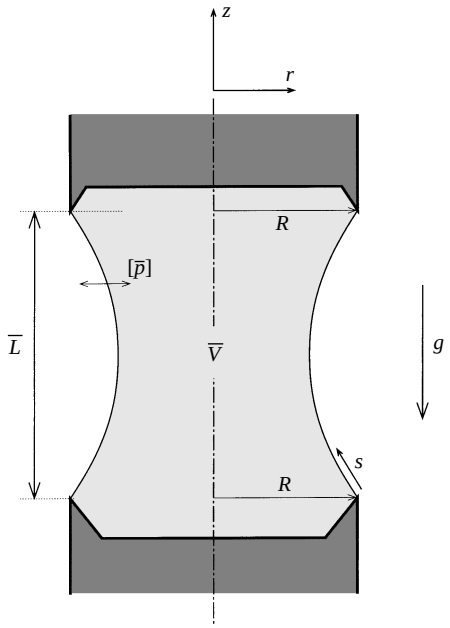


FIGURE 2. Liquid bridge with no flow; overbars denote dimensional quantities.

Here dot superscripts represent derivatives by arclength in the $(r, z)$-plane. $\bar{\kappa}_0$ is the curvature at position $z = 0$. Lengths have been non-dimensionalized by the bound radius $R$, and pressure jump at the interface $[p]$ is non-dimensionalized by $\sigma/R$ where $\sigma$ is the surface tension (figure 2). The hydrostatic pressure head is given in terms of Bond number, the ratio of gravitational to surface forces:

$$B \equiv \frac{gR^2\Delta\rho}{\sigma}. \tag{3.3}$$

Here $g$ is gravity and $\Delta\rho$, density difference, is counted positive for a heavy bridge.

The boundary conditions for the system of 2nd-order equations (3.2) are,

$$\left.\begin{array}{ll} r(0) = 1, & r(S) = 1, \\ z(0) = 0, & z(S) = L, \end{array}\right\} \tag{3.4}$$

where $S$ is total arclength in the $(r, z)$-plane, and $L$ is the dimensionless length of the liquid bridge. The reduced volume of the liquid bridge is given by

$$V = \frac{1}{L}\int_0^S r^2\dot{z}\,\mathrm{d}s, \tag{3.5}$$

where $V = 1$ for a cylinder. A *shape deviation* from the cylinder may be defined in terms of total arclength, as

$$\varepsilon \equiv ((S/L)^2 - 1)^{1/2}, \tag{3.6}$$

where $\varepsilon = 0$ for a cylinder and $\varepsilon > 0$ for a non-cylindrical shape.

It is known that there is at most one stable solution for a given set of parameters $\{B, V, L\}$. The boundary of stability is shown in figure 3*a* in the $(V, L)$-plane for various $B$. States inside the envelope are stable. The $B = 0$ stability limit is classical (cf. Gillette & Dyson 1971 for a modern treatment). In figure 3*a*, solid lines represent instability to axisymmetric (various $B$) and dotted lines to non-axisymmetric

disturbances (only $B = 0$). Stability limits for $B \neq 0$ have been determined by Meseguer (1983) for axisymmetric disturbances and more recently by Slobozhanin & Perales (1993) for arbitrary disturbances, applying variational characterizations presented by Myshkis *et al.* (1987). The cylindrical liquid bridge is a solution for all $L$ provided $\{B, V\} = \{0, 1\}$, but it is stable only for $L < 2\pi$. There are no stable bridges having $\{B, V\} = \{0, 1\}$ for $L > 2\pi$. The various bifurcations that occur along pieces of the boundary are discussed in Lowry & Steen (1995*b*). Gravity is a uniformly destabilizing force. Figure 3*b* shows the effect of gravity on the PR limit in the $(L, B)$-plane ($V = 1$) which is singular at $\{B, L\} = \{0, 2\pi\}$.

### 3.2. *Flow case*

This section lays a basis for reporting the experimental observations. An upward axial flow imposed on the liquid bridge modifies both shape and stability. For a cylindrical volume, an infinite core–annular rod flow with no net flow in the bridge is a first approximation, obtainable in closed form. The interface between fluid A (imposed flow) and fluid B (induced bridge flow) is an infinite cylinder in that approximation, equivalent to assuming large surface tension ($\sigma \to \infty$ or $|C| \ll 1$). The flow has a different constant pressure gradient in each phase, giving rise to a *differential* pressure gradient $[p_z]$ at the interface. A capillary number may be defined in terms of this gradient,

$$C \equiv \frac{[p_z]R^2}{\sigma}. \tag{3.7}$$

In terms of the inner (connector rod) and outer(tube) radii, $R_i$ and $R_o$, the viscosity ratio, $\mu_A/\mu_B$, and the total forced volumetric flow rate, $Q$, the differential pressure gradient has the form

$$[p_z] = f(R_i/R, R_o/R, \mu_A/\mu_B)\ \frac{\mu_A Q}{R^4}. \tag{3.8}$$

where the function $f$ is available (for the approximation) in closed form but is not needed below. It follows that

$$C \propto \frac{\mu_A Q}{\sigma R^2}. \tag{3.9}$$

The flow-rate $Q$ is measured directly in the experiments while $C$ is used in the plots below. From equation (3.7), and taking the dimensionless form, the pressure jump due to flow is

$$[p] = [p]_0 + Cz. \tag{3.10}$$

Here, $[p]_0$ is the pressure jump at position $z = 0$. When gravity also acts, this pressure adds to the hydrostatic pressure head of equation (3.1) to give a combined pressure,

$$[p] = [p]_0 - (B - C)z. \tag{3.11}$$

Equation (3.11) suggests the interpretation of $(B - C)$ as an *effective* Bond number and forms the basis for the empirical determination of $C$ from $Q$ (cf. §4).

For flowing systems, the Young–Laplace equation may not be adequate, however. The general normal stress boundary condition states that $\bar{\kappa} = \boldsymbol{n} \cdot \boldsymbol{T}_{AB} \cdot \boldsymbol{n}$, where $\boldsymbol{T}_{AB}$ is the tensorial jump in stress at the interface, and $\boldsymbol{n}$ is the outward normal to the surface. The resulting curvature profile, $\bar{\kappa}(z)$, is a pointwise measure of the jump in stress along the liquid bridge.

The contribution of the flow to the curvature profile can be identified. In cylindrical coordinates, the jump in normal stress at an axisymmetric interface between fluid A

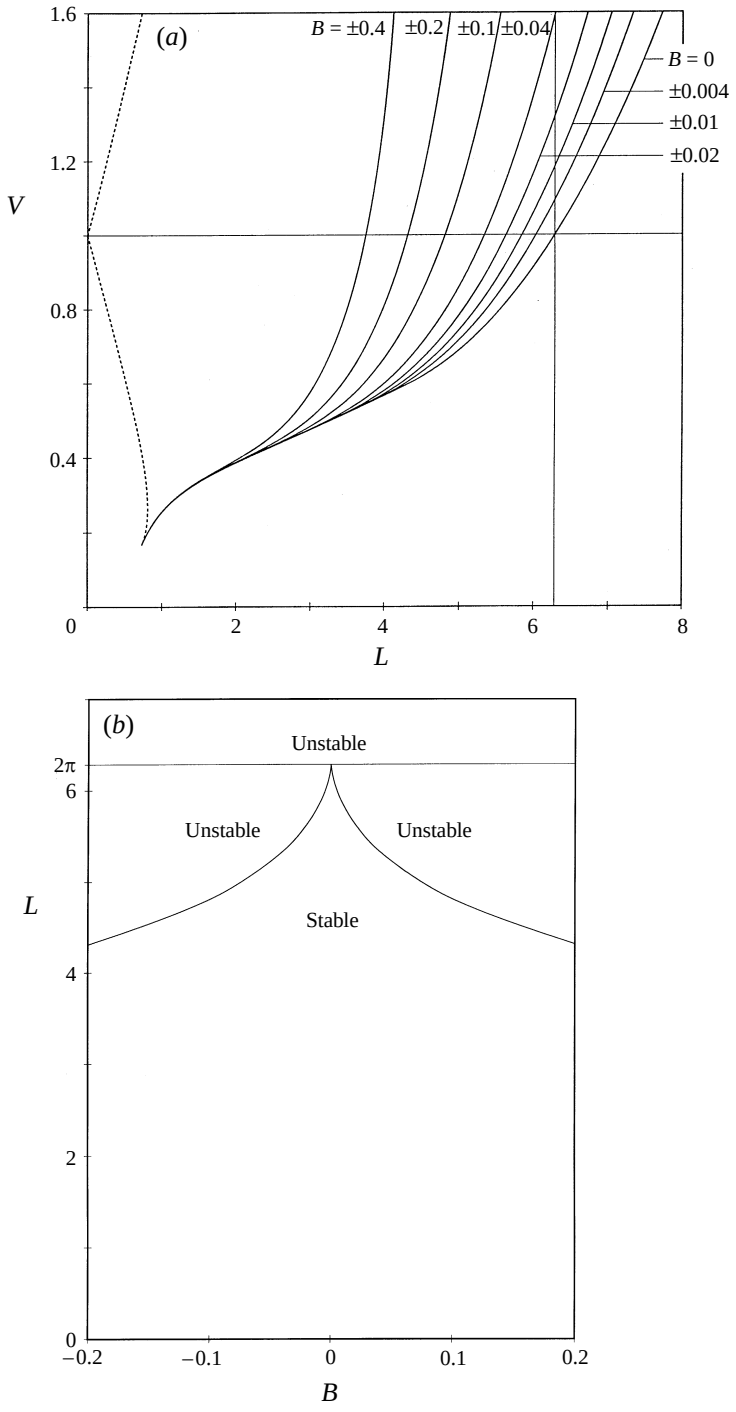


FIGURE 3. (*a*) Stability boundaries for bridge with no flow and (*b*) dependence of critical length on Bond number ($V = 1$).

and fluid B can be written (see the Appendix),

$$\boldsymbol{n}\cdot\boldsymbol{T}_{\mathrm{AB}}\cdot\boldsymbol{n} = [p] - (2+4\dot{r}^2\dot{z}^2)\left[\mu\frac{\partial v_n}{\partial n}\bigg|_{\mathrm{B}} - \mu\frac{\partial v_n}{\partial n}\bigg|_{\mathrm{A}}\right]. \tag{3.12}$$

Here $v_n$ is the component of velocity normal to the interface and $n$ represents the normal direction. Of course, in the absence of flow, only the first term on the right survives – the Young–Laplace equation is recovered. The additional term, attributed to a combination of flow and deformation, can be written in terms of a pressure gradient,

$$[\hat{p}_z] \equiv \frac{\mathrm{d}}{\mathrm{d}z}\left\{(2+4\dot{r}^2\dot{z}^2)\left[\mu\frac{\partial v_n}{\partial n}\bigg|_{\mathrm{B}} - \mu\frac{\partial v_n}{\partial n}\bigg|_{\mathrm{A}}\right]\right\} \tag{3.13}$$

so that

$$\frac{\mathrm{d}\bar{\kappa}}{\mathrm{d}z} = [p_z] + [\hat{p}_z]\,. \tag{3.14}$$

Equation (3.13) identifies one of two contributions to the slope of the curvature profile (3.14), and is useful in interpreting the profile. The deviatoric part is small when the flow is nearly rectilinear (i.e. a nearly cylindrical interface). However, under conditions that give a stagnation point on the interface, there may be a strong extensional component to the flow and $[\hat{p}_z]$ may be significant. In such cases and others, definition (3.7) must be reinterpreted since $[p_z]$ is no longer a constant, or even approximately so.

## 4. Liquid selection and measurement issues

The radius of the main rod, $R = 7.05$ mm, and the outer tube, $R_o/R = 2.13$ are fixed for the results reported below. The radius of the inner connecting rod is $R_i/R = 0.532$, unless otherwise noted.

The Plateau chamber relies on a small density difference $\Delta\rho$ between bridge and bath liquids. Plateau balanced the density of an oil with an aqueous alcohol mixture by tuning the mixture. Similar pairs of liquids are still used in present day Plateau chambers. A typical balance with such a pair is $\Delta\rho \approx 10^{-3}$ g cm$^{-3}$. Lowry (1996*a*) has shown that tuning isomeric or homologous organic compounds to the density of pure water can reduce $\Delta\rho$ by an order of magnitude. Isomeric mixtures of 2-fluorotoluene (2-FT), 3-fluorotoluene (3-FT), and 4-fluorotoluene (4-FT), which straddle the density of water, are used in the experiments. A second system, chlorocyclohexane (CCH) and chlorocyclopentane (CCP), with greater viscosity than the fluorotoluenes, is used in a few of the runs. The water employed is purified by reverse osmosis and filtered to remove particulate matter down to 0.2 μm.

The choice of isomeric and homologous mixtures eliminates (essentially) the density change with time due to compositional change that is typical of aqueous alcohol mixtures. On the other hand, density change with time due to temperature change remains an issue. The coefficients of thermal expansion of bridge and bath liquids are on the order of $10^{-4}$ g cm$^{-3}$ K so that control of density balance to $10^{-4}$ g cm$^3$ requires temperature control to better than 1°C (uniformly in space and time). This factor limits the density balance in our apparatus, especially in the dynamic mode where the bridge is continuously exposed to over 100 l of water during a typical experimental run (about 5 hours). The importance of temperature control in a Plateau situation has been recognized (Carruthers & Grasso 1972).

Accurate measurement of small density differences is difficult using conventional techniques. We employ an indirect method. The density difference, which varies from experiment to experiment depending on mixture composition, can be inferred from shape measurements in the no-flow case. Actually, it is the *ratio* of density difference to surface tension (or $B$) that can be inferred from comparison with the well-established no-flow theory. One approach, for bridges of cylindrical volume, measures the length at which it breaks, $L_c$, and compares with the prediction of destabilization by $B \neq 0$ (figure 3*b*). Another method fixes length, records the bridge image for a series of volumes including the cylindrical volume, and compares with shapes predicted by theory (cf figure 10*a*). A more precise method is also used (cf figure 9*a*): Bond number is measured from the slopes of curvature profiles in the no-flow case (equation (3.1)). The latter methods have been compared elsewhere (Lowry & Steen 1995*a*).

Interfacial tension $\sigma$ must also be measured by an indirect method since shape methods depend on a known density difference. Our approach uses a series of fluorotoluene/toluene and chlorocyclohexane/cyclohexane mixtures and extrapolation. These mixtures have densities significantly different from that of water, so that the difference can be measured with a hydrometer. The surface tensions is then determined by shape analysis. By extrapolating to zero percent toluene or cyclohexane, the surface tensions for pure fluorotoluene and chlorocyclohexane in water are recovered: $\sigma_{2\text{–FT/H}_2\text{O}} = 0.033 \pm 0.002$ N m$^{-1}$; $\sigma_{\text{CCH/H}_2\text{O}} = 0.026 \pm 0.001$ N m$^{-1}$.

To determine the capillary number, the pressure gradient due to flow $[\hat{p}_z]$ is needed. This can be measured by differentiating the curvature profile, if available, knowing the hydrostatic gradient (cf equation (3.14)). It can also be measured indirectly by establishing a correlation between $C$ and flow rate, based on the observation that flow can cancel density difference (cf equation (3.11)). Specifically, given a cylindrical volume, the cylindrical shape occurs if and only if the pressure gradient vanishes. By determining the flow rate at which a bridge of known density imbalance $B$ becomes cylindrical, a capillary number is established (i.e. $C = B$ at that flow rate). A plot of $C$ against $Q$ is determined in this way. The relationship is linear as expected for bridge flows that are creeping flows or nearly rectilinear flows, consistent with expression (3.9). The slope gives an empirical evaluation of the constant of proportionality in (3.9).

Viscosity of the bridge liquid is measured using a Cannon-Fenske routine viscometer for a variety of compositions of 2-FT/4-FT and CCH/CCP mixtures (see Lowry 1996*a*). The viscosity of 2-FT/4-FT is $\sim 0.65$ mPa s, and of CCH/CCP mixtures at the density of water, $\sim 1.6$ mPa s.

Image analysis is the basis of two of three measures of bridge response. Images provide axisymmetric bridge profiles as $r = f(z)$ data sets. Accurate approximation of the total arclength $S$ of the profile is used to measure the deviation in shape from the cylinder, $\varepsilon$ (equation (3.6)). Volumes can be measured to comparable accuracy via equation (3.5). Less accurate, but perhaps more valuable information, is the distribution of azimuthal curvatures along the profile. An algorithm that calculates azimuthal curvature directly from the digitized image has been developed. This is not a curve fit to a family of predicted shapes but uses kernel estimation of derivatives to give the curvature profile for an arbitrary shape. The method has been tested extensively for profiles in the range of interest, important given the dangers of twice differentiating a noisy representation of a curve. The method is described in detail elsewhere (Lowry 1996*b*).

## 5. Theoretical framework

Stability analysis of a full two-fluid model with flow is not practical, in view of the non-trivial geometry and finite interface. The predictions of a one-fluid model will serve as a framework. Volumes are restricted to $V = 1$. The action of the outer pipe flow is modelled as a shear stress applied to the interface that is pinned at its ends. The flow field within the bridge is calculated using the lubrication approximation (justified by $L/(R-R_i) \approx 13$) and assuming a uniform applied stress. Since the actual shear distribution on the interface is not constant, a quantitative comparison cannot be expected. Details of the calculation are reported elsewhere (Chen & Steen 1994).

The result of the weakly nonlinear analysis is a bifurcation equation,

$$0 = \tfrac{1}{2}\lambda\varepsilon + \tfrac{3}{32}\,\varepsilon^3 + (B - \alpha C) + \beta C\varepsilon^2. \tag{5.1}$$

Here, $\lambda \equiv (L-2\pi)/(2\pi)$ is the primary parameter and represents distance from the PR limit. Coefficients $\alpha$ and $\beta$ depend on $R_i/R$ in a way predicted by the model. However, in experiments reported below, it is useful to interpret $\alpha$ and $\beta$ as also accounting for the differences in the definition of $C$ between the model (which uses shear stress) and experiment (which uses equations (3.7) and (3.8), or expression (3.9)).

Figure 4(*a*) plots equation (5.1) for $B = C = 0$, the unperturbed pitchfork, illustrating the PR limit. Here deflection $\varepsilon$ is positive for bulge-down and negative for bulge-up. Note that this is a slightly different definition than for shape deviation. Figure 4(*b*) shows the imperfect bifurcation that appears when up–down symmetry is broken by a heavy bridge, $B > 0, C = 0$. In contrast (figure 4*c*), $B = 0, C > 0$, shows how flow from bottom to top also breaks symmetry but with an interface deflection of opposite sign.

The pitchfork is a codimension-2 bifurcation. Density imbalance and flow are two independent parameters whose effect on the interface deflection can counterbalance one another. If the two effects are combined in just the right proportion, it is possible that the first-order effects exactly cancel, leaving higher-order effects to determine the behaviour, as illustrated by the transcritical bifurcation in figure 4(*d*). Note that, according to figure 4(*d*), (i) a perfectly cylindrical bridge can exist right up to the PR limit, and (ii) slightly non-cylindrical bridges are stable for lengths *beyond* the PR limit. Of course, the transcritical bifurcation itself (codimension-1) is susceptible to symmetry-breaking and the two qualitatively different results of breaking are shown in figure 4(*e*, *f*). In one case (figure 4*f*), a small island of stable length beyond the PR limit is created and, in the other case (figure 4*e*), the short region of stabilized bridge remains connected to the family of stable equilibria below the PR limit.

This theory gives mathematical flesh to the above physical argument motivating study of the singularity. In fact, the experiments reported here were done before the solution of the one-fluid model was available.

## 6. Results

For the case of no flow, measurements of shape deviation and curvature profiles are found to be in agreement with predictions of theory. For low flow rates, as measured by $C$, shapes and curvature profiles show deviation that is linear in $C$. For larger flow rates, nonlinear effects are observed. In the linear regime, when flow acts against gravity but does not overcome it ($C < B$), the shape of liquid bridges is in agreement with that determined by the effective Bond number, $B-C$. When capillary number is sufficiently small ($C <\sim 0.01$), the critical length is also determined by the

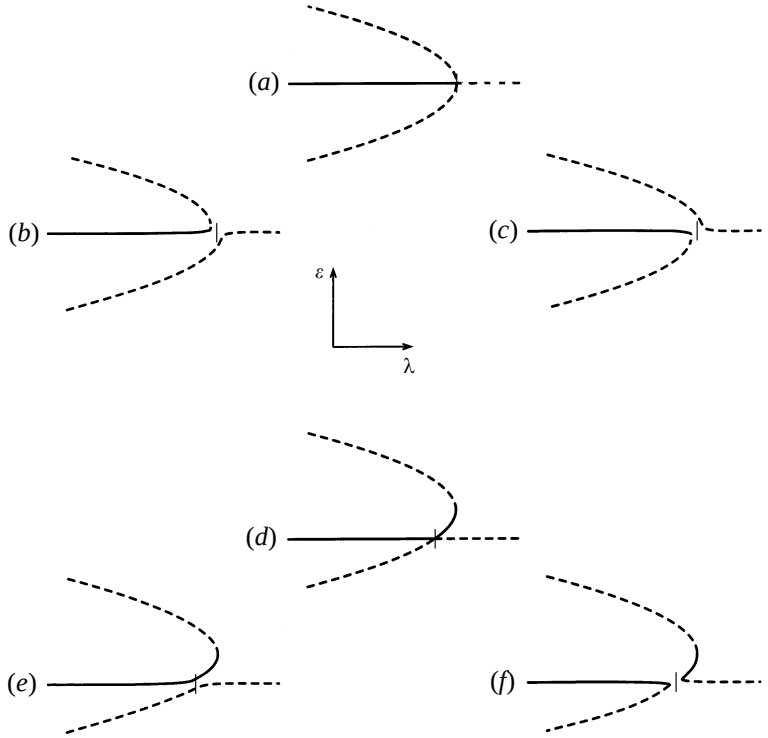


FIGURE 4. Unfolding of the PR pitchfork bifurcation (solid lines are stable, dotted lines unstable states): (*a*) pitchfork ($B = C = 0$), (*b*) perturbed by heavy density imbalance ($B > 0, C = 0$), (*c*) perturbed by flow from bottom to top ($C > 0, B = 0$), (*d*) perturbed by the 'cylindrical' flow rate ($B = C \neq 0$), (*e*) perturbed diagram (*d*) ($B \neq C > 0$) and (*f*) a different perturbed diagram (*d*) ($B \neq C > 0$).

effective Bond number. Hence, over a small range of flows which counter gravity, the static theory of liquid bridges may be adapted to account for flow effects. When flow overcomes gravity or acts in the same direction ($0 < B < C$ or $B < 0 < C$), the effect of flow is much stronger than the effective Bond number would indicate, as evidenced by larger deviations in shape and a sharp decrease in stability with increasing flow.

The effects of flow on shape are apparent from images of the bridges. When $B > 0$ and there is no flow, a near-cylindrical liquid bridge bulges downward slightly. An upward flow can balance gravity and the cylindrical shape is recovered while further increasing flow causes the bridge to bulge slightly upward. For the latter, shape deviations are larger than would be expected based on the effective Bond number. Nearer $L_c$, stabilization accompanies the shape change. The sequence on decreasing flow rate is illustrated in figure 5. A bridge may be cylindrical and stable in the presence of flow (figure 5*a*), but unstable (broken) when there is no flow (figure 5*c*). With a flow rate in between, it is bulged down (figure 5*b*).

### 6.1. *Behaviour near collapse*

Three kinds of collapse have been observed. The simplest and most common for near-cylindrical volumes is shown in figure 5(*c*). An axisymmetric disturbance grows until the bridge separates into two volumes by contact of the interface with the centre rod. In contrast, a stripping collapse is distinguished by a blob of fluid being detached from the rod and being carried away downstream. Axisymmetric and

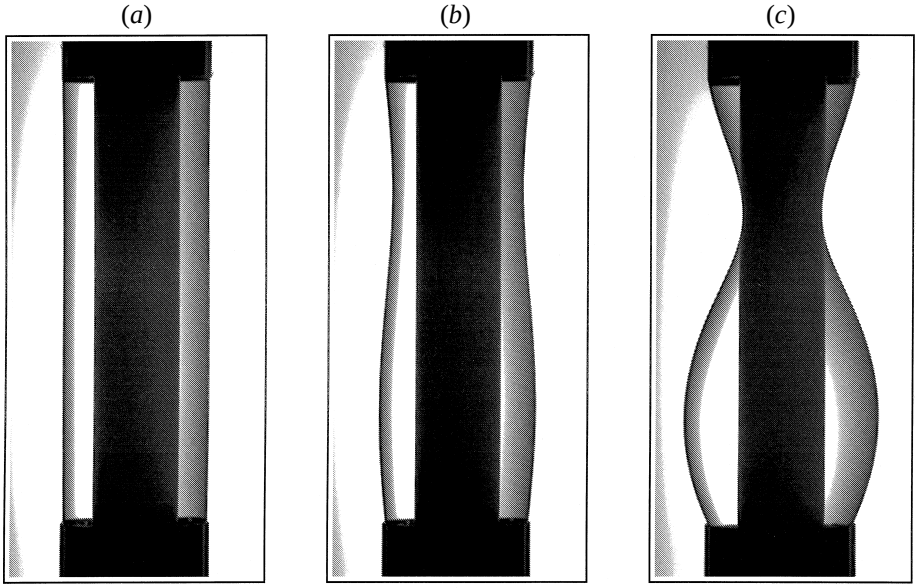


FIGURE 5. Images of CCH/CCP liquid bridges from PhotoCD, with $L = 6.088$, $V = 0.9995 \pm 0.0012$, $B = 0.0068 \pm 0.0005$, and (*a*) $C = 0.0094$, (*b*) $C = 0.0030$, (*c*) $C = 0$ (98.8% CCH, 1.2% CCP, $T = 19.75$°C).

non-axisymmetric stripping have been observed. In the non-axisymmetric version, a bulge forms and rotates around the axis of symmetry, growing in amplitude until it is stripped from the bridge by the flow.

The distinction between non-axisymmetric and axisymmetric collapse may be quantified in terms of shape deviation from the cylinder. Figure 6 shows the influence of flow on shape deviation. For short bridges ($L < 4$), no matter what the volume, flow has little effect on the shape (figure 6*a*). Flow rate was increased to the limit of capability of our apparatus and no collapse was observed, except for the largest volume ($V = 1.524$). There, a sudden non-axysymmetric stripping occurs. The non-axisymmetric bulge grows and rotates at a frequency of about once per second. Growth continues until the bulge breaks from the bridge and is swept downstream. The remaining bridge volume undergoes a quasi-static collapse. Note that no change in slope of deviation against $C$ is apparent near instability.

For longer bridges ($L > 5$), the collapse is generally axisymmetric. Figure 6(*b*) shows how flow monotonically increases the deformation of a slightly buoyant bridge until collapse, for all volumes. The instability apparently occurs at a turning point,

$$\frac{\mathrm{d}\varepsilon}{\mathrm{d}C} \to \infty.$$

Similar collapse behaviour is seen for heavy bridges (figure 6*c*, *d*), with an added feature that collapse may also occur upon decreasing flow rate (figure 6*d*, $V = 1.06$). This is possible whenever flow stabilizes a bridge that is otherwise unstable. In summary, the bridge breaks axisymmetrically at turning points with a few exceptions, notably for low-volume bridges (e.g. figure 6*b*, $V = 0.837$; figure 6*c*, $V = 0.818$). In the low-volume cases the central rod may influence the equilibria near collapse.

Axisymmetric collapse is either 'quasi-static' or 'stripping'. At lower flow rates, the bridge bulges at one end and necks at the other, and collapse is a slow steady

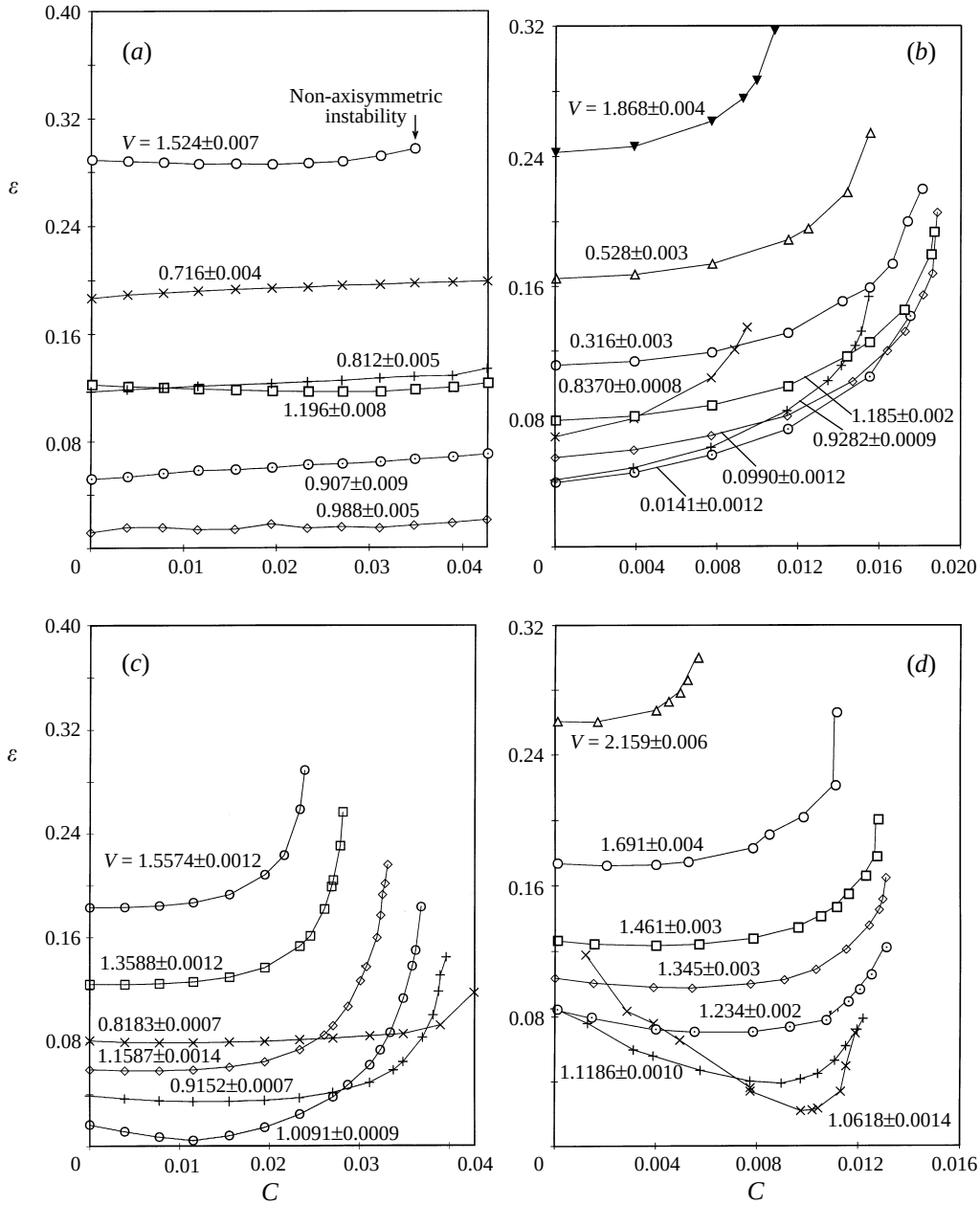


FIGURE 6. Dependence of deviation on capillary number for various volumes for (*a*) $L = 2.834$, (*b*) $L = 5.376$ with $B = -0.0008 \pm 0.0003$ (91.6% 4-FT, 8.4% 2-FT, $T = 20.10°$C) and for (*c*) $L = 4.646$, (*d*) $L = 6.099$ with $B = 0.0080 \pm 0.0005$ (80% 4-FT, 20% 2-FT, $T = 19.95°$C).

increase in amplitude until the bridge becomes disconnected ('quasi-static'). As flow rate and/or bridge length increase there is a change from this sort of collapse to the stripping type of catastrophic breakage.

Collapse always results in a discrete change in shape deviation. However, the approach to collapse distinguishes the 'pitchfork' from the 'turning point' collapse, as seen above. There are strict parallels of these instabilities with those seen in static

bridges ($B \neq 0$). The turning point is a common stability limit for short to moderate length bridges for volumes near unity (Lowry & Steen 1995*b*) while a pitchfork bifurcation to non-axisymmetry is apparently common for larger volume (or heavier) bridges. Slobozhanin & Perales (1993) have studied the effects of Bond number on the onset of non-axisymmetry (for the static case) and found that it occurs at $B \sim 1$ for $V \sim O(1)$. An analogous instability due to flow seems to occur at much smaller effective Bond numbers. A bulge-growth instability from a very rotund static bridge ($V - 1 \gg 1$) has also been documented (Russo & Steen, 1986).

The three types of collapse all occur when the approach to instability involves a quasi-static change of some control parameter. All appear to be analogous to static collapse in terms of the cause of instability. In contrast, a sudden change in flow rate or bridge length can lead to an oscillating collapse. When there is a narrow range of flow rates over which a bridge is stable it collapses upwards at one limit and downwards at the other. Altering parameters suddenly past the stability limit appears to give rise to oscillations between the two limiting states, now unstable. In extreme cases the oscillation is observed to pause for over a second at one of the unstable states before collapse proceeds to completion. In no case were stable oscillations observed. All observed stable equilibria were stationary in shape.

### 6.2. *Curvature profiles*

Curvature profiles $\bar{\kappa}(z)$ remain linear but increase in slope with increasing flow rate in the regime where flow acts as a linear addition to gravity (figure 7). This is expected from $\bar{\kappa} = \bar{\kappa}_0 - (B - C)$, obtained by substituting curvature for pressure in equation (3.11). The value of $\bar{\kappa}_0$ is determined by the volume of the bridge (constant volume constraint) and hence is independent of flow.

Curvature profiles from several experiments where $0 < C < B$ confirm the linear change of slope and pivoting about a near constant $\bar{\kappa}_0$. Consider figure 7(*a*). The data have been restricted to lower flow rates to emphasize this linear change. The slope of the curvature profile varies monotonically from negative slope with no flow ($C = 0$) to positive slope with flow. Deviations near the boundaries (and possibly some non-linearity) are likely artifacts of the image analysis method. These effects are amplified in longer bridges (figure 7*b*). Although error bars strictly depend on shape, the shaded region shown in figure 7(*a*) is typical of profiles reported here.

The slope of a curvature profile (via linear least squares) represents an *apparent* Bond number for a given liquid bridge, $B_a$. Ideally, $B_a = B - C$. The dependence of apparent Bond number on flow rate when flow counters gravity ($0 < B$) is shown in figure 8(*a*). The point at which the apparent Bond number is zero lies within the linear region when the Bond number is sufficiently small. The linearity is also present when gravity and flow act in the same direction ($B < 0$), although to a lesser extent, as illustrated in figure 8(*b*). At higher flow rates the curvature profiles are no longer linear (mentioned above), as indicated by increasing errors in the determination of slope (where errors are not indicated, they are smaller than the symbols on the graphs). The loss of linearity appears to coincide closely with significant nonlinearities relative to the linear $C = 0$ profiles. In other words, when the effect of $C$ on $B_a$ becomes nonlinear at higher flow rates, the curvature profiles also become nonlinear.

The slope of the curve $B_a(C)$ is less than unity in the linear regime, so that $B_a = B - \gamma C$ with $\gamma < 1$. This is likely due to the boundaries of the bridge which dampen the induced return flow and thus weaken the normal stresses there. However, as the curvature profiles are unreliable at the bounds, it is not possible to determine

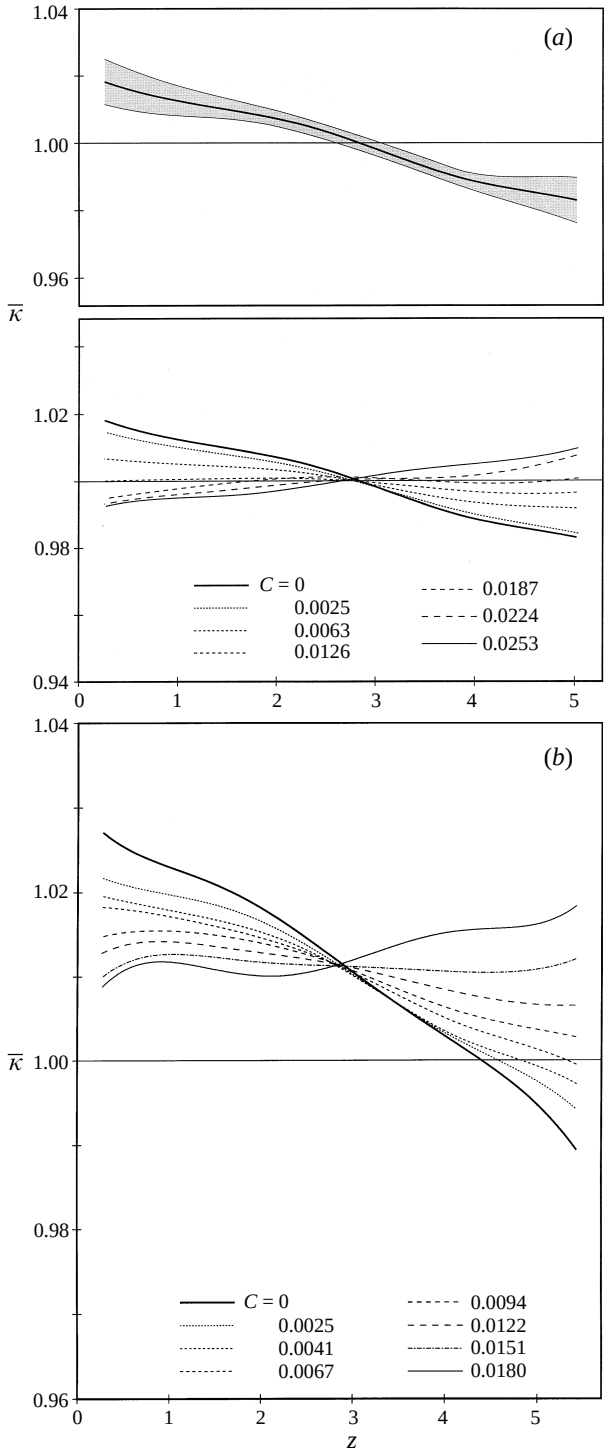


FIGURE 7. Curvature profiles showing effects of small axial flows with $B = 0.0068 \pm 0.0005$ and (*a*) $L = 5.361$, $V = 1.0013 \pm 0.0010$, (*b*) $L = 5.725$, $V = 0.9777 \pm 0.0005$ (98.8% CCH, 1.2% CCP, $T = 19.75°$C).

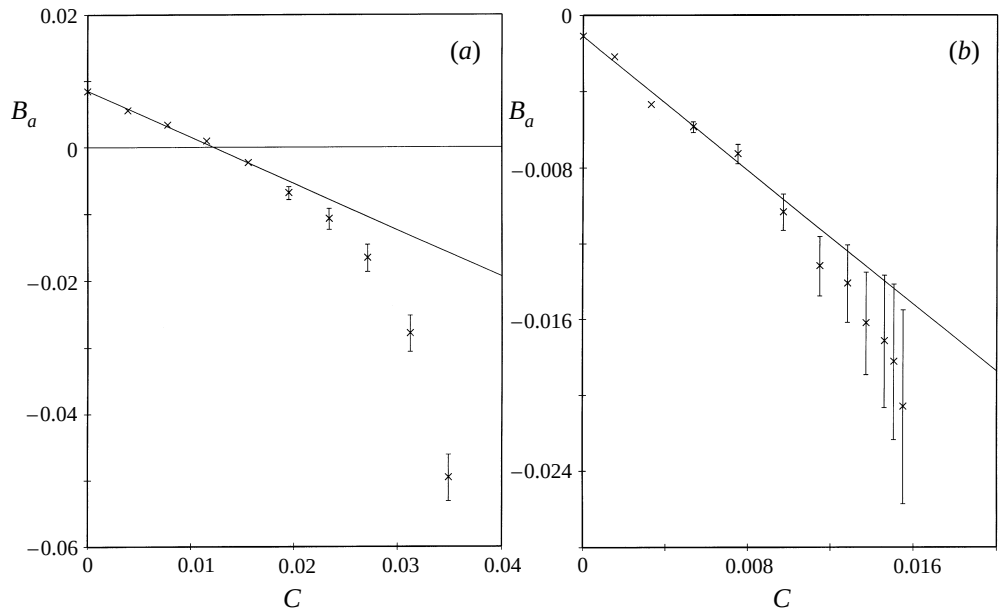


FIGURE 8. Dependence of apparent Bond number on capillary number (*a*) with $B = 0.0080 \pm 0.0005$, $L = 4.646$, $V = 0.9758 \pm 0.0007$, (80% 4-FT, 20% 2-FT, $T = 19.95°\text{C}$), and (*b*) with $B = -0.0008 \pm 0.0003$, $L = 5.376$, $V = 1.003 \pm 0.003$, (91.6% 4-FT, 8.4% 2-FT, $T = 20.10°\text{C}$).

the effects of turning flows directly. In any case, $\gamma < 1$ suggests that the one-fluid model (finite interface) may do a better job of capturing flow-induced pressure than the two-fluid approximation with cylindrical shape (infinite interface).

When $B < C$, the tendency is for the liquid bridge to bulge at the top and neck at the bottom. For small-amplitude deviations from a near-cylinder the bulging and necking have no net effect on the flow. However, at larger amplitude the bulge has a disproportionately large effect as it acts to block the forced flow of water. The blocking of the return flow by the neck is comparatively minor as that flow is indirectly forced. The asymmetry between the effects of bulge and neck are suggested by both the infinite core–annular rod flow (Lowry 1994) and flows with finite interface (Chen & Steen 1994). The result is that the curvature profile for larger $C$ shows a strong rise upstream of the bulge, and a smaller rise near the neck. Figure 9 shows two sets of corresponding shape and curvature profiles: zero flow (figure 9*a*) and maximum flow (figure 9*b*). A relatively small blockage of the outer flow forces a disproportionately large stress response (figure 9*b*). Further increase in flow rate leads to larger bulges and curvatures and eventually the bridge becomes unstable to the axisymmetric stripping mode of collapse. Figure 9 also illustrates that curvature profiles are a more sensitive measure of flow than shape profiles.

### 6.3. *Shape deviations*

Deviations from the cylindrical shape, $\varepsilon$, determined by image analysis may be directly compared with the deviation computed for static equilibria. In these experiments $V$ was varied with $L$ held constant. $B$ was estimated from the flow rate required to form cylindrical bridges, as outlined above.

Figure 10 illustrates the reduction of deviation by axial flow. Figure 10(*a*) shows the no-flow case for reference. The gravity imbalance $B = 0.008$ breaks the symmetry and

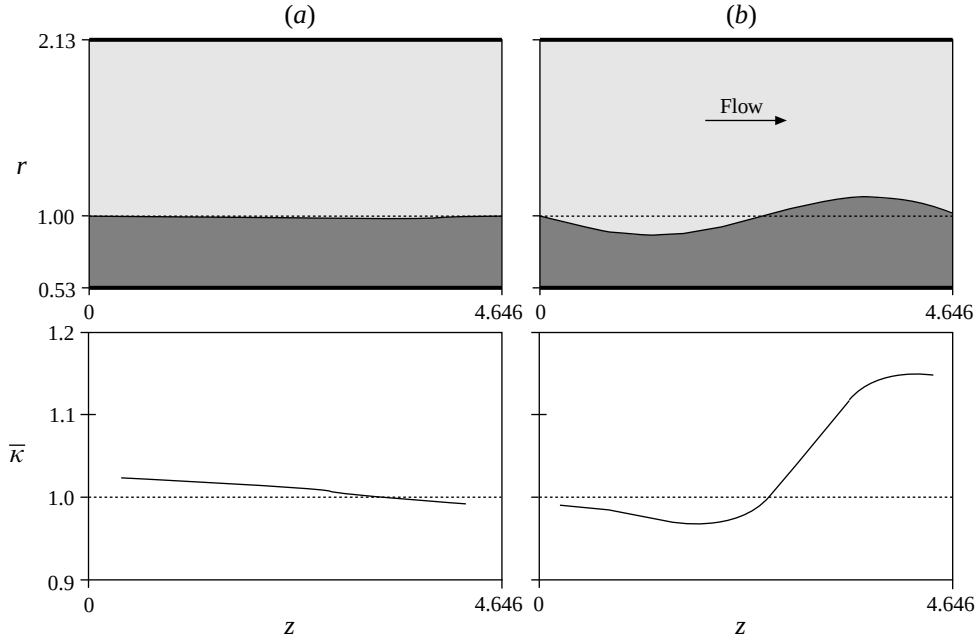


FIGURE 9. Interfaces (top) and curvature profiles (bottom) showing nonlinear axial flow effects with (*a*) $C = 0$, and (*b*) $C = 0.0349$ (80% 4-FT, 20% 2-FT, $T = 19.95°$C).

precludes cylindrical shapes even for cylindrical volumes. The discrepancy between the two sets of data (increasing and decreasing volume) is likely due to Bond number drift with time. Figure 10(*b*) shows the effect of increasing the flow until the effective Bond number is near zero. With a balanced flow ($B \approx C$), deviation from the cylinder is significantly reduced.

Figure 11(*a*) illustrates the effects of flow on a bridge with $L > 2\pi$, and the same $B$ as figure 10 ($0 < C < B$). Note that $V > 1$ for this bridge. Figure 11(*b*) shows the extreme sensitivity to flow rate near the stability limit ($B \approx C$). A change in capillary number of only 0.0001, the difference between the two runs, results in a significant shift in the position of the minimum. There is an asymmetry in the response to flow near $B = C$. The response to flows with $C < B$ is generally linear, while for $C > B$ there is a strongly nonlinear response which leads to highly non-cylindrical shapes. The strength of this nonlinear response increases as volume increases.

In an alternative measure of the influence of flow, shape deviation is observed while $V$ is fixed and $C$ is varied. Results of figure 6 were discussed in §6.1. For $B > 0$, deviation can be reduced by flow for near-cylindrical volumes. Flow has the most significant effect on shape near stability limits and on near-cylindrical shapes, and the least effect on short liquid bridges and rotund liquid bridges away from stability limits.

### 6.4. *Maximum length*

The effect of flow on maximum length of liquid bridges with cylindrical volumes is examined. Bond number was estimated from the critical length, $L_c$, at which a liquid bridge becomes unstable and broken in the absence of flow (cf. figure 3*b*). Volume during these experiments was controlled visually to be $V = 1$. Errors in volume of up to 2% were determined afterward by image analysis. Hence, the relation shown

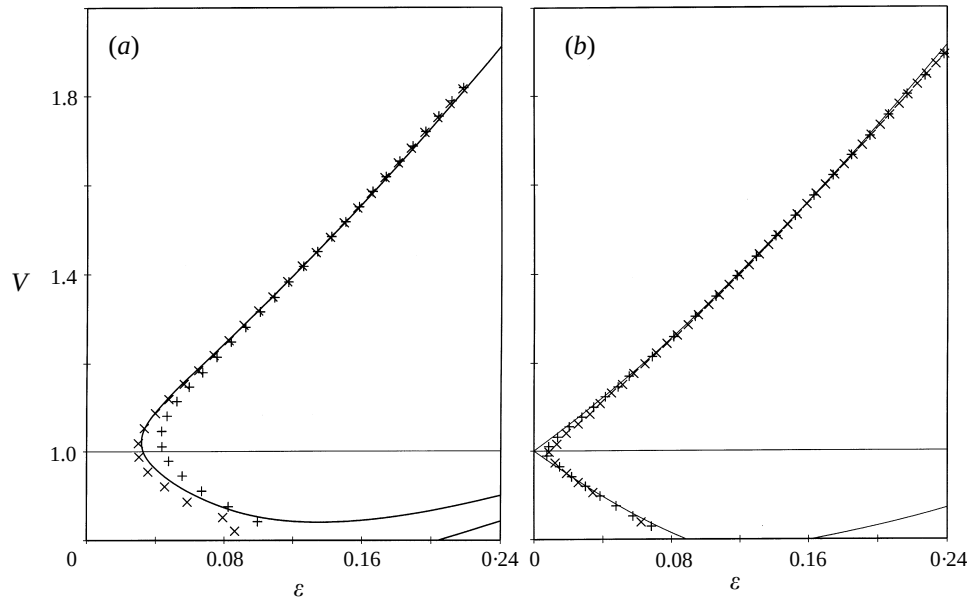


FIGURE 10. Shape deviations from image analysis with $L = 5.409$, and (*a*) $C = 0$, $B = 0.008$ (two runs), (*b*) $C = 0.0075, B = 0$, with comparison to computed equilibria (solid curves) (70% 4-FT, 30% 2-FT, $T = 20°$C).

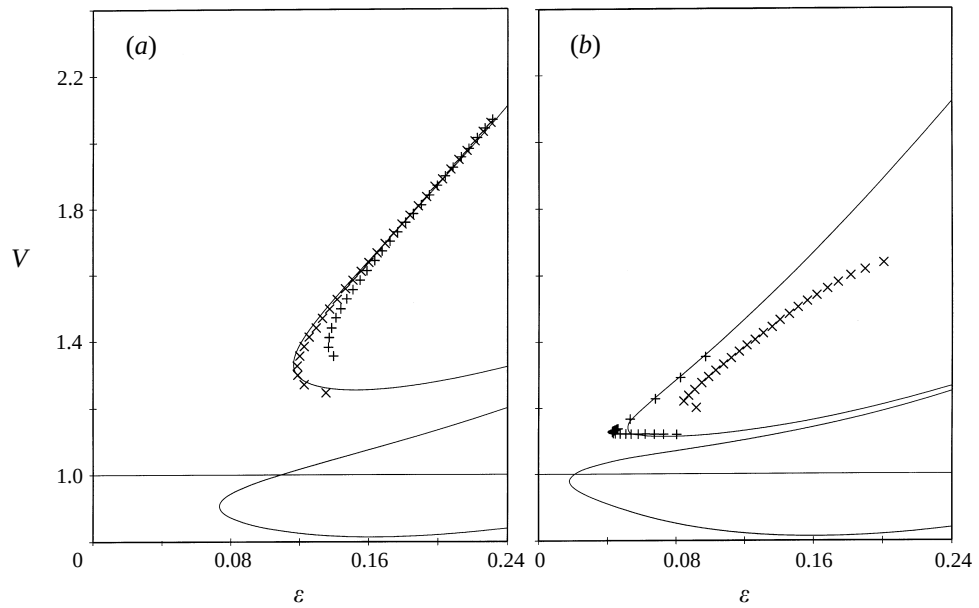


FIGURE 11. Shape deviations from image analysis with $L = 6.498$, (*a*) $C = 0$, $B = 0.008$, (two runs), (*b*) $C = 0.0088, B = -0.001$ (two runs), with comparison to computed equilibria (solid curves) (70% 4-FT, 30% 2-FT, $T = 20°$C).

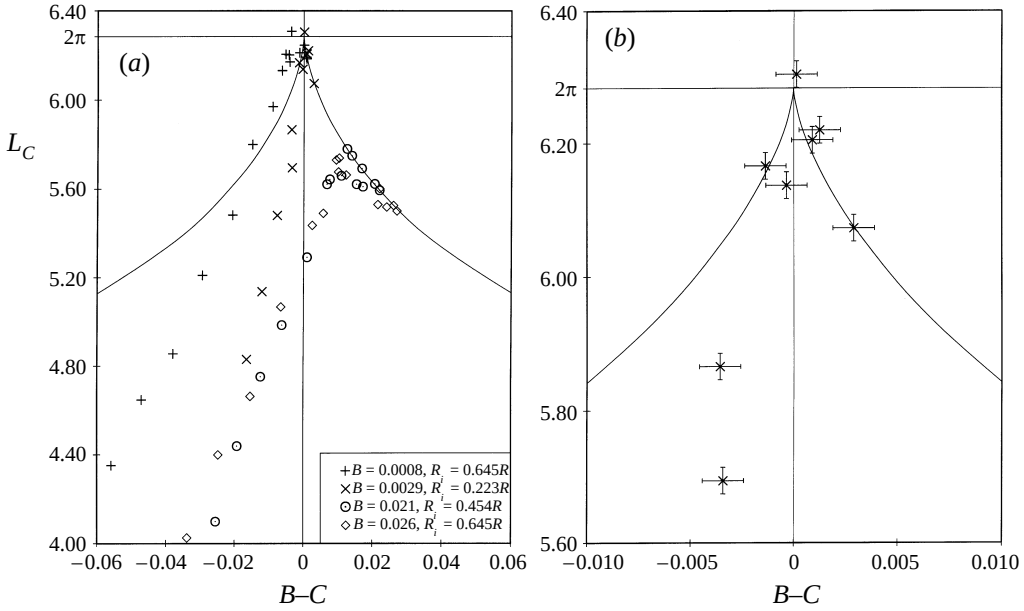


FIGURE 12. (*a*) Dependence of maximum stable liquid bridge length on $B - C$ for $V = 1.00 \pm 0.02$ and $0 < B < 0.04$ with comparison to static $L_c(B)$ curve, (*b*) detail of (*a*) near PR limit (FT mixtures, $T = 20°\text{C}$).

in figure 3(*b*) was not used directly as in general $V \neq 1$. However, the no-flow correction is available (Perales, Meseguer & Martinez 1991) and was applied to this set of experiments (Lowry 1994). On one hand, these data are readily compared to the static theory but, on the other hand, they are more prone to error since $L$ and $V$ are varied simultaneously.

The four series of experiments represented in figure 12(*a*) begin by measuring maximum length in the absence of flow, the rightmost data point in each set. The bridge is then reinstated by shortening it, after which the flow rate is increased. A new maximum length is measured and so forth. Some stabilization is observed in all cases. For small Bond numbers, $B < 0.04$, it was experimentally possible to achieve an effective Bond number of zero. For the smallest $B$, lengths very near and perhaps beyond the PR limit are recorded. For moderate $B$ the maximum stabilized length did not reach the PR limit. For both small and moderate $B$, the stabilization never yielded a length extension of more than 4% beyond the maximum static length ($C = 0$). For flow rates higher than that, beyond the point of maximum length, there is a sharp decline in stability. The decline in length is roughly linear in flow rate. As was the case for shape deviation, there is an asymmetry in the response to flow. At low flow rates there is stabilization, in agreement with that predicted by the effective Bond number, but past the peak there is a strong destabilization with increasing flow. A closer examination of one stability peak shows that this asymmetry in response is also present close to the maximum stable length (figure 12*b*). This is in qualitative agreement with equation (5.1).

When Bond number is large enough that an effective Bond number of zero is not possible due to flow limitations in the apparatus ($B > 0.04$), two types of response to flow are observed (figure 13). The prevalent type is analogous to cases with smaller Bond number, where there is some stabilization followed by a sharp decline

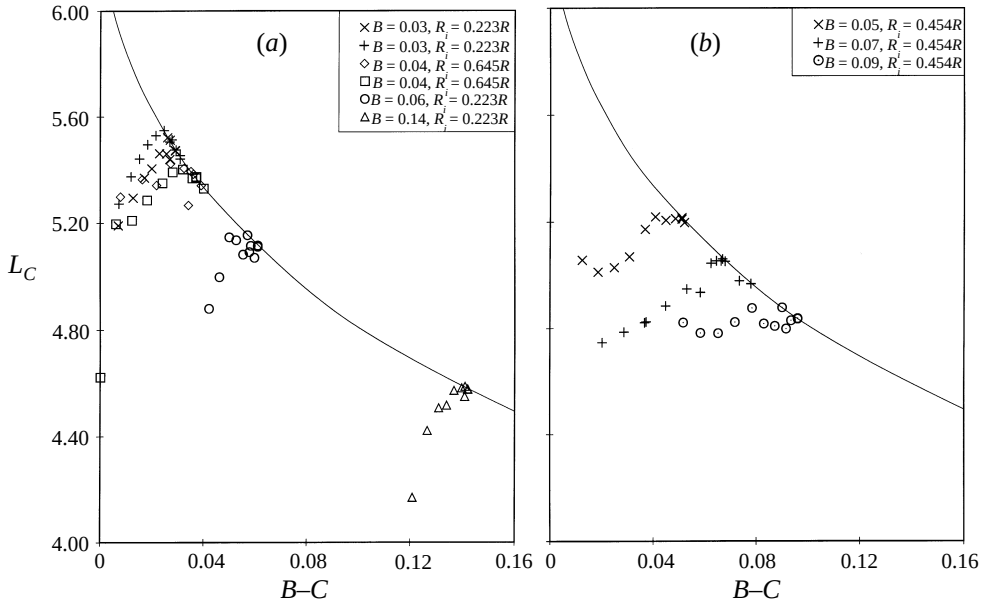


FIGURE 13. Dependence of maximum stable liquid bridge length on $B - C$ for $V = 1.00 \pm 0.02$ and $B > 0.04$: (*a*) typical, and (*b*) atypical with comparison to static $L_c(B)$ curve (FT mixtures, $T = 20°\text{C}$).

in maximum stable length (figure 13*a*). In contrast, in three sets of experiments, there is no sharp decline in stability with increasing flow (figure 13*b*). In one case, there is no significant change in stability within the range of capillary numbers possible. In these three cases the flow effects which cause destabilization appear to be partially absent. There also appears to be some correlation between large rod diameter and the decrease in destabilization.

### 6.5. *Maximum flow rate*

A more reliable and reproducible measure of the limit of stability is the maximum $C$ at which a bridge of fixed $L$ and $V$ is stable. The flow rate is increased until a bridge becomes unstable, and the volume prior to instability is determined via image analysis from video. An interesting finding is that, for bridges near the PR limit, there is both a maximum and minimum flow rate for stability. In other words, flow generates an island of stability that would not otherwise exist.

For short bridges with no gravity to balance ($B \approx 0$), the stability limit is nearly linear in $C$, as for $L = 4.65$ in figure 14(*a*). As $L$ increases destabilization of low-volume bridges increases. This indicates interaction of the flow and the minimum volume stability limit (static theory), which occurs at increasingly large volumes as length increases. For $L = 5.376$ and $B = 0$, this limit occurs at $V = 0.762$, according to static theory. At volumes slightly above this limit, the flow destabilizes the liquid bridge when it pushes a small excess of liquid to the top of the bridge, leading to an axisymmetric quasi-static collapse. At large volumes ($V >\sim 1.4$), the bulge at the top of the bridge due to flow is large enough that axisymmetric stripping occurs. The maximum stability in terms of capillary number is attained where necking does not destabilize the bridge significantly and yet where volume is small enough that the bulge of the bridge is not large.

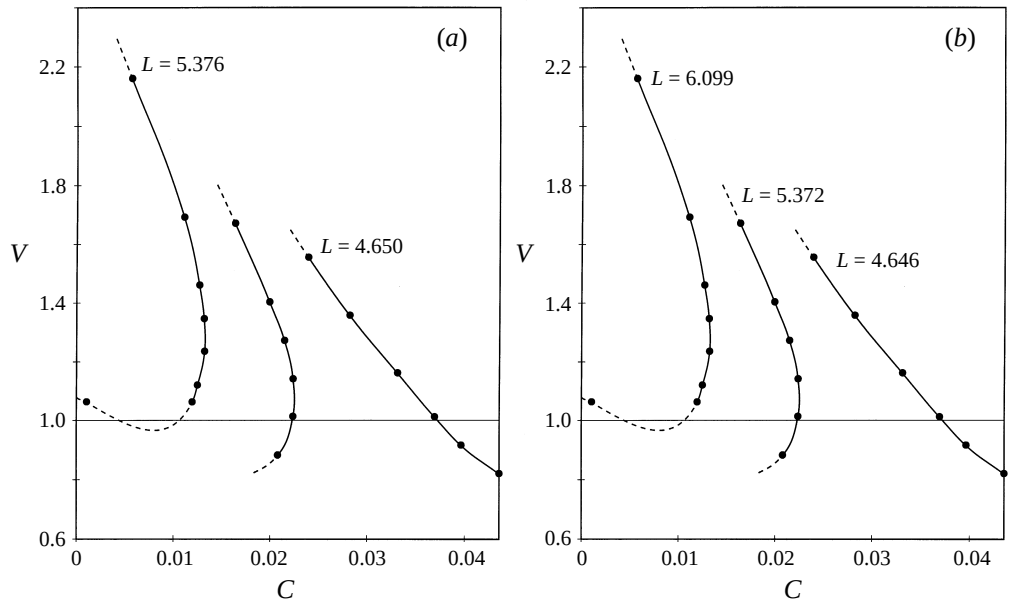


FIGURE 14. Liquid bridge stability limits in terms of volume and capillary number: (*a*) $B = -0.0008 \pm 0.0003$ (91.6% 4-FT, 8.4% 2-FT, $T = 20.10°$C, (*b*) $B = 0.0080 \pm 0.0005$ (80% 4-FT, 20% 2-FT, $T = 19.95°$C).

The effects of balancing gravity with flow can be observed in a moderate flow with a small Bond number (figure 14*b*). At the greatest length, flow stabilizes bridges which are otherwise unstable. Cases have been observed where the range of stability in terms of capillary number is smaller than 0.001, both for near-cylindrical and non-cylindrical volumes. Figure 15 shows curvature profiles for one such case (the bracketing capillary numbers are very near to the stability limits). The profiles appear to indicate that the cause of instability is not the significant change in stress distribution seen for instability at shorter lengths and larger capillary numbers (cf. figure 9*b*). This suggests a quasi-static collapse, as there is also no singularity in stress (pressure) in the static case. To further corroborate this interpretation, where there are small ranges of stability, the bridge collapses, bulging downwards at the lower flow limit, while at the upper limit, it collapses upwards. One would expect this with a purely gravitational instability with change in sign of the density difference.

## 7. Discussion

The well-developed $B = C = 0$ theory provides a means for interpreting observations in the linear regime. For $|B - C| < 10^{-2}$ and arbitrary $V$, the static theory reasonably accounts for the bridge shape in the presence of flow, at least in the sense of average shape given by deviation $\varepsilon$. For $|V - 1| \ll 1$, the linear curvature profiles confirm that flow-induced pressure is a linear modification of the hydrostatic gradient for $|B - C| < 10^{-2}$, although the linear regime is a bit larger for counterflow as compared to coflow. Nonlinear curvature profiles develop quickly as flow is increased beyond $C \approx 10^{-2}$ due to deformation that constricts the annular cross-section of flow. These results might have been anticipated, although the narrowness of the range of linear behaviour perhaps comes as a surprise.

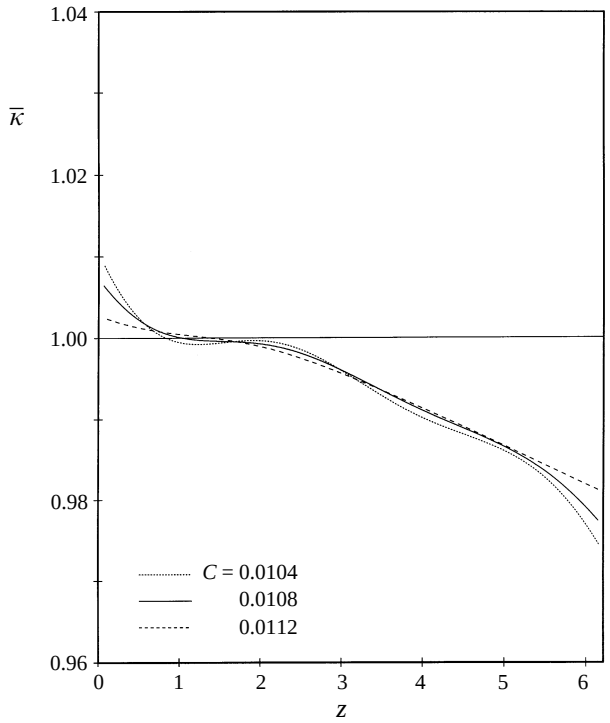


FIGURE 15. Curvature profiles showing variation with capillary number near stability limits with balancing flow ($B = C$), $L = 5.376$, $V = 1.0120 \pm 0.0008$, $B = 0.0068 \pm 0.0005$ (98.8% CCH, 1.2% CCP, $T = 19.75°C$).

In contrast, the influence on the stability limits (maximum length or maximum flow rate) shows nonlinear behaviour. The nonlinear effects are most noticeable for small density imbalance, lengths near critical, and volumes near cylindrical. Key observations suggest that (i) lengths beyond the PR limit may be possible with flow (cf. figure 12*b*), (ii) islands of stability can be induced by flow for bridges that are otherwise unstable (cf. figure 14*b*), and (iii) increasing flow rate can decrease shape deviation before the ultimate increase that occurs with the approach to axisymmetric instability (cf. figure 6*d*).

Consider figure 12(*a*) to illustrate how the results may be interpreted in terms of the schematics of figure 4. For all $B$, increasing $C$ from zero increases the stability limit at least initially. This corresponds to starting with figure 4(*b*) (the stability limit is the turning point) and deforming towards diagram 4(*d*). Clearly, the turning point approaches the PR limit and can in fact exceed it as illustrated by figure 4(*d–f*). This explains the small-$B$ data beyond the PR limit in figure 12. On the other hand, note that in an experiment the order in which the control parameters are adjusted may be crucial especially if one lands in parameter space of figure 4(*f*). It is likely to be tricky to access the island of stability beyond the PR limit.

For larger $B$, the increase in $L_c$ with increasing $C$ is very limited (figure 12*a* and figure 13*b*). The fall-off can be explained by a bluff-body creeping-flow pressure effect. For cylinders, the flow-induced pressure effect is stabilizing. However, if the initial deflection is sufficiently large (large $B$), low flow will initially reduce the deflection by means of the superposed axial gradient until, with greater flow, destabilizing gradients due to deflection of the streamlines dominate.

The island of stability seen in figure 14(*b*) can be explained by equation (5.1). Furthermore, the turning points of figure 6 are also captured by equation (5.1) and are thus similar to the turning point limits of figure 4.

Figure 4 also puts the role of density imbalance in some perspective. Suppose a perfect balance were achieved for every experiment ($B = 0$). Then flow could only be destabilizing. Even though the PR limit could be achieved in the absence of flow, in principle, bridges beyond the PR limit would be unstable. Density imbalance is not only advantageous but necessary to reach states beyond the PR limit. The codimension-2 nature of the subcritical pitchfork gives an additional independent control parameter and thus provides access to a greater range of nonlinear behaviour. We remark that this nonlinear stabilization concept has also been predicted for the Rayleigh–Taylor instability in two contexts: a two-dimensional slot (Chen & Steen 1996*a*) and a Hele-Shaw thermal cell (Chen & Steen 1996*b*). In both cases, tilt angle and flow-induced pressures are the competing perturbations.

## 8. Conclusions

The linear and nonlinear effects of axial flow on liquid bridges have been observed. They are perturbations of the static liquid bridge system. In the linear regime, at low flow rates ($C < B$), shape and stability behave like a static bridge subject to an effective Bond number, $B - C$. When Bond number is sufficiently small, the destabilization and shape changes caused by gravity can be removed by applying a balancing flow ($B = C$). In this manner, flow can be used to negate gravity.

In the nonlinear regime, flow and gravity compete more subtly. At flow rates ($B < C$), the flow is generally destabilizing although there are circumstances where this effect is minimal, apparently. The destabilization is accompanied by a significant change in liquid bridge shape, caused by an increase in downstream pressure. The asymmetry of the response to inward necking versus outward bulging reflects the stabilizing influence of flow. Flow modifies the liquid bridge shape and opens the possibility of stabilization beyond the PR limit. Two linearly destablizing effects, gravity and flow, can be arranged to cancel one another, in which case the remaining nonlinear effect becomes dominant. In accordance with the framework supplied by the one-fluid model, and the associated unfolding (equation (5.1)), the nonlinear effect is responsible for the observed stabilization of bridges shorter than the PR limit and the corresponding diagrams are a guide to nonlinear stabilization beyond the PR limit.

Direct experimental evidence of a bridge with $L > 2\pi$ is ambiguous (cylindrical volume). Yet all the observations fit the framework of equation (5.1) which also predicts stabilization beyond the PR limit. This framework further suggests why experiments are likely to be ambiguous. First, it is only possible to stabilize incrementally beyond the PR limit and, second, this window of stabilization may only be reachable by a specific protocol of control parameters.

B.J.L. thanks NSERC for a PGS fellowship. The authors gratefully acknowledge support by NASA grants NAG3-801 and NAG3-1401.

## Appendix

The jump in normal stress at an interface is (using $\boldsymbol{n} = \dot{z}\boldsymbol{e}_r - \dot{r}\boldsymbol{e}_z$)

$$\boldsymbol{n} \cdot \boldsymbol{T}_{\mathrm{AB}} \cdot \boldsymbol{n} = [p] + \dot{z}^2\tau_{rr} - 2\dot{r}\dot{z}\tau_{rz} + \dot{r}^2\tau_{zz}, \tag{A 1}$$

where the deviatoric stress $\tau_{ij} = \boldsymbol{e}_i \cdot (\boldsymbol{T}_{\mathrm{AB}} - [p]\boldsymbol{I}) \cdot \boldsymbol{e}_j$ and $\boldsymbol{I}$ is the identity tensor. The stress components are related to velocity gradients by

$$\left.\begin{aligned} \tau_{rr} &= -2\mu \frac{\partial v_r}{\partial r}, \\ \tau_{zz} &= -2\mu \frac{\partial v_z}{\partial z}, \\ \tau_{rz} &= \mu \left( \frac{\partial v_r}{\partial z} + \frac{\partial v_z}{\partial r} \right). \end{aligned}\right\} \tag{A 2}$$

These can be transformed to derivatives tangent and normal to the surface using the equations

$$\left.\begin{aligned} v_r &= \dot{r} v_t + \dot{z} v_n, \\ v_z &= \dot{z} v_t - \dot{r} v_n, \end{aligned}\right\} \tag{A 3}$$

where $v_n$ is velocity normal (outward) to the surface, and $v_t$ is velocity tangent to the surface; and

$$\left.\begin{aligned} \frac{\partial}{\partial r} &= \dot{r} \frac{\partial}{\partial s} + \dot{z} \frac{\partial}{\partial n}, \\ \frac{\partial}{\partial z} &= \dot{z} \frac{\partial}{\partial s} - \dot{r} \frac{\partial}{\partial n}. \end{aligned}\right\} \tag{A 4}$$

Here, partial derivatives in $s$ and $n$ represent changes tangent and normal to the surface, respectively. The surface is impenetrable, so that

$$v_n \equiv 0 \tag{A 5}$$

holds everywhere on the surface. Equation (3.12) follows, by substitution of equations (A 2)–(A 5) into (equation A 1).

## REFERENCES


Carruthers, J. R. & Grasso, M. 1972 Studies of floating liquid zones in simulated zero gravity. *J. Appl. Phys.* **43**, 436–445.

Chen, Y.-J. & Steen, P. H. 1994 Influence of flow on interface shape stability. *Proc. 14th IMACS World Congress, Atlanta, GA, July*, 629–632.

Chen, Y.-J. & Steen, P. H. 1996*a* Suppression of the capillary instability in the Rayleigh-Taylor slot problem. *Phys. Fluids* **8**, 97–102.

Chen, Y.-J. & Steen, P. H. 1996*b* Stabilizing interfaces of finite extent with flow induced by thermal convection. In *Advances in Multi-Fluid Flows* (ed. Y. Renardy, A. Coward, D. Papageorgiou & S.-M. Sun), pp. 211–218. SIAM.

Gillette, R. D. & Dyson, D. C. 1971 Stability of fluid interfaces of revolution between equal solid circular plates. *Chem. Engng J.* **2**, 44–54.

Lowry, B. J. 1994 Shape stability of slender liquid bridges in axial flows. PhD dissertation, Cornell University.

Lowry, B. J. 1996*a* Density matching with water using mixtures of organic isomers and homologues. *Exps. Fluids* (in press).

Lowry, B. J. 1996*b* Pressure and stress measurement via image analysis (P-SIA) of axisymmetric drops and liquid bridges. *J. Colloid Interface Sci.* **178**, 284–297.

Lowry, B. J. & Steen, P. H. 1994 Stabilization of an axisymmetric liquid bridge by viscous flow. *Intl J. Multiphase Flow* **20**, 439–443.

Lowry, B. J. & Steen, P. H. 1995*a* Flow-influenced stabilization of liquid columns. *J. Colloid Interface Sci.* **170**, 38–43.

Lowry, B. J. & Steen, P. H. 1995*b* Capillary surfaces: stability from families of equilibria with application to the liquid bridge. *Proc. R. Soc. Lond.* A **449**, 411–439.

MESEGUER, J. 1983 The influence of axial microgravity on the breakage of axisymmetric liquid bridges. *J. Cryst. Growth* **62**, 577.

MYSHKIS, A. D., BABSKII, V. G., KOPACHEVSKII, N. D., SLOBOZHANIN, L. A. & TYUPTSOV, A. D. 1987 *Low-gravity Fluid Mechanics*. Springer.

PERALES, J. M., MESEGUER, J. & MARTINEZ, I. 1991 Minimum volume stability limits for axisymmetric liquid bridges subject to steady axial acceleration. *J. Cryst. Growth* **110**, 885.

PLATEAU, J. 1863 Experimental and theoretical researches on the figures of equilibrium of a liquid mass withdrawn from the action of gravity. *Annual Report of the Board of Regents of the Smithsonian Institution*, pp. 207–285.

PLATEAU, J. 1873 *Statique Expérimentale et Théoretique des Liquides Soumis aux Seules Forces Moléculaires*. Gauthier-Villars.

RUSSO, M. J. & STEEN, P. H. 1986 Instability of rotund capillary bridges to general disturbances: experiment and theory. *J. Colloid Interface Sci.* **113**, 154–163.

SLOBOZHANIN, L. A. & PERALES, J. M. 1993 Stability of liquid bridges between equal disks in an axial gravity field. *Phys. Fluids* A **5**, 1305–1314.